7/19/92 (2)

PREPARED FOR THE U.S. DEPARTMENT OF ENERGY,
UNDER CONTRACT DE-AC02-76-CHO-3073

PPPL-2856
UC-420,421,427

PPPL-2856

TRANSPORT OF ENERGETIC IONS BY LOW-*n* MAGNETIC PERTURBATIONS

BY

H.E. MYNICK

OCTOBER, 1992

PPPL PRINCETON PLASMA PHYSICS LABORATORY

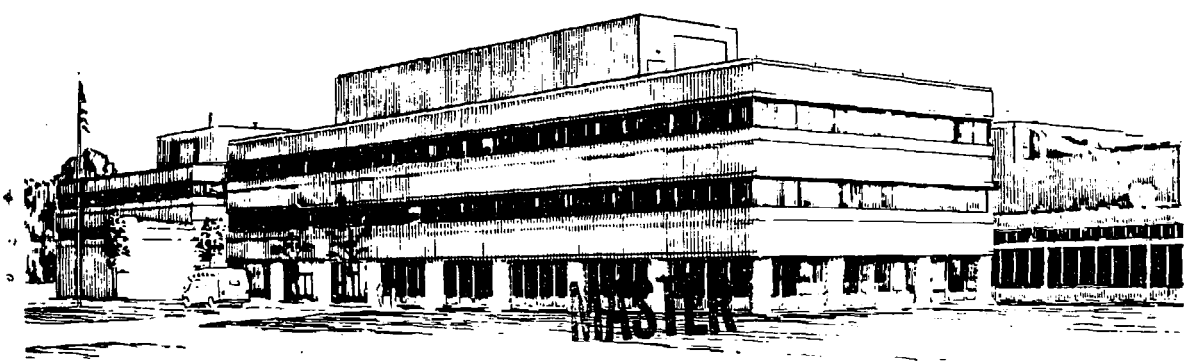

PRINCETON UNIVERSITY, PRINCETON, NEW JERSEY

PPPL--2856

DE93 002633

Transport of Energetic Ions by Low-n Magnetic Perturbations

H.E.Mynick
Plasma Physics Laboratory, Princeton University
Princeton, New Jersey 08543, U.S.A.

Abstract

The stochastic transport of MeV ions induced by low–n magnetic perturbations is studied, focussing chiefly on the stochastic mechanism operative for *passing* particles in *low* frequency perturbations. Beginning with a single–harmonic form for the perturbing field, it is first shown numerically and analytically that the stochastic threshold of energetic particles can be much lower than that of the magnetic field, contrary to earlier expectations, so that MHD perturbations could cause appreciable loss of energetic ions without destroying the bulk confinement. The analytic theory is then extended in a number of directions, to clarify the relation of the present stochastic mechanism to instances already found, to allow for more complex perturbations, and to consider the more general relationship between the stochasticity of magnetic fields, and that of particles of differing energies (and pitch angles) moving in those fields. It is shown that the stochastic threshold is in general a nonmonotonic function of energy, whose form can to some extent be tailored to achieve desired goals (*e.g.*, burn control or ash removal) by a judicious choice of the perturbation. Illustrative perturbations are exhibited which are stochastic for low but not for high–energy ions, for high but not for low–energy ions, and for intermediate–energy ions, but not for low or high energy. The second possibility is the behavior needed for burn control; the third provides a possible mechanism for ash removal.

PACS #s: 51.10+y, 52:25.Fi, 52.55.Fa

I. Introduction

The confinement of fusion products and other energetic ions in tokamaks is an issue of major importance for the success of fusion reactors. Since the early '80 s it has been realized that internally induced, low-n magnetic perturbations such as fishbones[1,2] can substantially enhance the loss of energetic particles, but the full picture of the possible mechanisms for such loss is still developing. In contrast to the coherent, resonant loss induced by fishbones, the present work is principally concerned with diffusive, 'stochastic' loss induced by low-n perturbations. For some years it has been known that trapped ions can be diffusively transported by low-frequency perturbations[3,4] ($\omega \lesssim 10$ kHz), where the low ω is balanced against the low values of the toroidal precession frequency Ω_ζ for trapped particles in the primary resonance $\omega \simeq n\Omega_\zeta$. A zero–frequency special case of this is diffusive loss due to TF ripple,[5] for which the 'stochastic transport' mechanism was first studied. Recently, it has been found experimentally,[6,7] numerically[8] and analytically[9] that passing particles can be similarly transported by higher frequency ($\omega \sim 100$ kHz) perturbations such as TAE modes, where the much higher value of ω balances against $k_\| v_\|$ in the primary resonance $\omega \simeq k_\| v_\|$. Because of the primary resonance conditions holding in the two cases, an expectation has been that low frequency perturbations should be effective for trapped particles, and high frequency for passing ones. However, contrary to this expectation, it has been shown[10–12] that low-ω MHD can also induce stochastic transport in passing particles. The conclusion in Ref. 11 was that the stochastic threshold for MeV ions (3.5 MeV alphas and similar charged fusion products) was about the same as or higher than that for the

magnetic field itself, so that one would expect no stochastic MeV ion loss if the magnetic field were adequate to confine the bulk plasma. However, this contrasts with the recent observations with alpha/triton detectors on TFTR that, in the presence of low-frequency MHD, a triton flux phase–coherent with the MHD is observed, enhancing the total flux over its quiescent level by a factor of about 4.[13]

The present work contributes to this developing picture of stochastic transport in three general ways. First (Sec. II), we revisit the passing–particle, low-ω mechanism, beginning with a simple model MHD perturbation, having a single harmonic, with poloidal and toroidal mode numbers m and n. We show numerically and analytically that the conclusion of Ref. 11 that the stochastic threshold for MeV ions is comparable with or higher than the magnetic threshold is not generic, but that it is not difficult to find perturbations for which the opposite is true,[14] reinstating this mechanism as a possible explanation of the above–noted TFTR results.

Second (Sec. III), having developed an analytic understanding of numerical results manifesting this mechanism in the simplest single–harmonic case, the theory is generalized in a number of directions, unifying the theory for the present mechanism with ones studied earlier, and permitting consideration of the transport induced by more complicated magnetic perturbations. In addition to making contact with the TAE–mode case, the theory's generalization to arbitrary ω may also explain recent DIII-D observations[15] that, in the presence of intermediate frequency ($\omega \sim 30$ kHz) MHD activity, more MeV ions are expelled than can be accounted for by trapped particles alone.

And third (Sec. IV), the extended transport theory opens the possibility of an energy-selective transport mechanism, which one might impose

intentionally, which could be useful for suppression of undesired transport from internally–generated MHD, or for burn control and ash removal. From earlier work, intuitions have developed for whether more energetic particles should be transported more or less easily by a given perturbation spectrum. On the one hand, more energetic particles perform more 'orbit–averaging' over the structure of the perturbations inducing transport,[16] which often acts to *reduce* the transport induced by a perturbation of a given amplitude. This theoretical expectation is supported by experimental observations of transport rates of energetic electrons[17] and ions,[13] as well as by numerical simulations.[18] The conclusions of Ref. 11 are consistent with this picture. On the other hand, an opposite intuition exists, that the larger drifts of more energetic particles allow them to resonate with a larger range of perturbations, or sidebands of the same perturbation, causing *increased* transport, and lower stochastic thresholds, for more energetic particles. The trapped–particle stochastic ripple mechanism already mentioned is one example manifesting this tendency. Examples of both trends can be found in the transport induced by both turbulent[17] and ripple perturbations. The extended theory developed here provides a picture which unifies these two seemingly opposite trends, for transport due to low to moderate–n modes ($n \sim 1 - 20$), acting either individually, or in combination. The basic point is that stochasticity is not a monotonic function of energy, but rather is in general a nonmonotonic function which can have an appreciable amount of structure, whose specifics depend in detail on the set of perturbations present, in a manner which the extended theory makes explicit. Thus, it may be possible to 'design' perturbations which will be below stochastic threshold for both thermal particles and for alphas near their birth en-

ergy, but above threshold for alphas at intermediate energies where their removal is desirable. An initial exploration of these possibilities is presented in Sec. IV.

Finally, in Sec. V we give some summarizing discussion of the lessons learned from the earlier sections, and indicate some issues raised by the work for which further study seems desirable.

II. Single–Harmonic Perturbations

We begin by considering the motion of alphas in a single–harmonic model of an MHD perturbation, first numerically, and then analytically. The numerical results are generated by a guiding–center (gc) code in flux coordinates, developed from earlier implementations of such codes.[19,20] Following Ref. 2, we model the perturbing magnetic field $\delta\mathbf{B} = \nabla \times \delta\mathbf{A}$ by $\delta\mathbf{A} = \tilde{\alpha}\mathbf{B}_0 R_0$, with $\mathbf{B}_0$ the equilibrium magnetic field, R_0 the major radius at the magnetic axis, and $\tilde{\alpha}(\mathbf{x}, t)$ a function of real-space position $\mathbf{x}$ and time. The perturbing electric field $\delta\mathbf{E} = -c^{-1}\delta\dot{\mathbf{A}}$ is given directly from $\delta\mathbf{A}$, but is negligible for the low–frequency perturbations considered here. We parametrize $\mathbf{x}$ by the flux coordinates (r, θ, ζ), with minor-radial variable $r \simeq (2\psi/B_0)^{1/2}$, having value a at the plasma boundary, and constant on a flux surface, as is the toroidal flux $\psi(r)$. In terms of ψ and the poloidal flux function $\chi(r)$, $\mathbf{B}_0$ may be written

$$\mathbf{B_0} = \mathbf{B}_t + \mathbf{B}_p = \nabla\psi \times \nabla\theta + \nabla\zeta \times \nabla\chi.$$

The safety factor is $q(r) \equiv d\psi/d\chi$, which we model with the quadratic form $q(r) = q_0 + (q_a - q_0)(r/a)^2$.

A simple model of a single MHD mode is taking $\tilde{\alpha}$ to have a single helical component,

$$\tilde{\alpha}(r,\theta,\zeta) = \alpha(r) sin\eta, \tag{1}$$

with amplitude $\alpha(r)$ and mode phase $\eta = n\zeta - m\theta + \phi_{nm}$. ϕ_{nm} is an arbitrary mode phase, which may be given a time dependence $\phi_{nm} = \phi_{nm0} - \omega t$ if desired. However, the transit/bounce frequency Ω_b of an alpha (~ 1 MHz) is much larger than ω for the low-frequency of the modes of principal interest here. Thus, ϕ_{nm} is taken as a constant for the numerical results of this section, though for the analytic development we shall keep ω arbitrary, with an eye to the more general theory of Sec. III. We model α by

$$\alpha(r) = \alpha_{mx}(r/r_{mx})^m[(a-r)/(a-r_{mx})]^p,$$

which peaks at $r_{mx}/a = m/(m+p)$ with value α_{mx}, and yields radially global modes, scaling as r^m for small r (cf. Fig. 1). p is chosen so that the mode peaks in the vicinity of the mode rational surface $q_{nm} \equiv m/n$. An adequate simple choice is $p = n$ for $q_{nm} > 1$, and $p = 3n$ for $q_{nm} = 1$. This single-helicity form provides a simplest model problem for understanding the effects of low-n perturbations, and also captures much of the physics of the multiple-helicity case, needed for a full description of both the coupled-harmonic structure of a true toroidal eigenmode, as well as to study transport due to multiple modes. The theory is generalized to cover these cases in Sec. III.

With this form for the perturbation, the radial perturbing field is given by

$$\delta B_r \simeq -B_0 b(r) \sin\eta, \tag{2}$$

with amplitude $b(r) \simeq m\alpha/(r/R_0)$. Thus, for example, for a (2,1)-mode, at $r = r_{mx} = 2a/3$, one may convert from amplitude α_{mx} to $b_{mx} \equiv b(r_{mx})$ using $b_{mx} = 3\alpha_{mx}/\epsilon_a \simeq 8.3\alpha_{mx}$, where $\epsilon_a \equiv a/R_0$ is the inverse aspect ratio at $r = a$, and in the final form we have used TFTR parameters $a = 96$ cm, $R_0 = 262$ cm.

A perturbation of the form (2) produces magnetic islands at the $q = q_{nm}$ surface of half-width[20]

$$\delta r_{nm}/R = (4qb/nRq')^{1/2}. \tag{3}$$

In Fig. 2 are shown the poloidal projections of two characteristic orbits for alphas at birth energy $E = E_0 \equiv 3.5$ MeV using the TFTR parameters just noted, along with $q_0 = 1, q_a = 4, B_0 = 5$T, and a very large (2,1) perturbation ($\alpha_{mx} = 10^{-3}$), in order to emphasize its effects. The radius $r = r_{mx}$ is indicated by the inner dashed curve, the solid curve indicates $r = a$, and the outer dashed curve shows the position of the limiter. Fig. 2a shows a trapped particle, with pitch $\lambda \equiv v_{\|}/v = .18$ at launch point $(r/R_0, \theta) = (.15, -\pi/2)$, and Fig. 2b shows a passing particle, having $\lambda = .46$, with the same launch point. For the trapped particle (trapping-state index $\tau = 0$), one notes the wandering of the banana tip from bounce to bounce along the vertical line $R \simeq$constant until its escape to the wall. As noted in Sec. I, such transport for trapped particles is expected from earlier theories[3-5] on the effect of low-ω perturbations.

Somewhat more surprising is the (co-going) passing orbit ($\tau = 1$), which is also strongly affected by the perturbation, spiralling out to the wall in on the order of 10 transit periods for this amplitude of α_{mx}. The loss mechanism is insensitive to the relative mode-particle phase (cf.Figs 2b,3a and b), and

to the particle pitch (cf.Figs. 2b, 3c, and 3d). Moreover, the radial motion is not coherent in character, as occurs, for example, during trapped–particle expulsion by fishbones;[2] the bounce–averaged radius ('banana center') $\bar{r}$ does not vary in a regular sinusoidal fashion, and excursions in the bounce–averaged value $\bar{\eta}$ of the particle's phase in the mode are not bounded by 2π, as is the case for coherent, 'superbanana'-type motion. (We shall use the terms 'bounce–period,' 'bounce–average,' 'superbanana,' *etc.* here to apply to both passing as well as trapped particles. Both trapping states may be mathematically dealt with on the same footing, so it is convenient to use terminology compatible with this.)

Instead, the loss is the new instance of stochastic transport first identified in Ref. 10; in addition to the stochastic mechanisms for trapped particles in low-ω perturbations[3–5] and for passing particles in high-ω modes,[8] one sees that an analogous mechanism also holds for passing particles in low-ω perturbations. The mechanism is somewhat less intuitive from the reasoning based on the primary resonance condition, as discussed in Sec. I, but, as for the other two mechanisms, it is due to the overlap of multiple islands produced by a single perturbation, where successive islands satisfy the sequence of resonance conditions $\omega = n\Omega_\zeta + l_b\Omega_b \simeq k_\parallel v_\parallel + l\Omega_b$, for $l = 0, \pm 1, \pm 2, \ldots$ [For $\tau = 1$, $\Omega_\zeta \simeq v_\parallel/R \simeq q\Omega_b$ is again the bounce–averaged time–rate of change of ζ, and $l_b = l - m$ is the bounce–harmonic of the resonance in question.] This may be seen from the Poincare plots of Figs. 4a and b. Both are puncture plots at the $\zeta = 0$ surface using a $\delta\mathbf{B}$ generated by the (2,1) perturbation of Fig. 3, but for $\alpha_{max} = 10^{-4}$. Fig. 4a is the puncture plot for the magnetic field itself or, equivalently, for alphas with vanishingly small energy and $\lambda = 1$, which simply follow field lines. Fig. 4b is the same plot, but

for alphas at $E = E_0/2$, and again with $\lambda = 1$. As expected, Fig. 4a shows an $m = 2$ island around the $q = 2$ surface. Comparing this with Fig. 4b, one notes two principal differences arising when the drifts are turned on. First is a shift of the $m = 2$ island toward the outboard side, which occurs simply because of the outward shift of co-going orbits, and because resonance for these occurs for $q_d \equiv \Omega_b/\Omega_\zeta$, differing somewhat from $q = 2$ due to the particle drifts in a flux surface. Second, and of central importance here, is the appearance of an *additional* ring of islands, of symmetry $m = 3$, occurring around the $q_d = 3$ surface. As α_{mx} increases from its value in Fig. 4 toward that in Figs. 2 and 3, the width of these two island rings increase toward each other, until at an intermediate, threshold value α_{st} the islands overlap, and the observed stochastic loss of the orbits ensues. At the same time, one notes that the magnetic plot remains unstochastic, contrary to the situation investigated in Ref. 11, whose magnetic map manifested multiple islands. Which magnetic structure is actually more typical in the presence of low-n MHD is unclear. While the usual theoretical expectation for a toroidal eigenmode involves a superposition of poloidal harmonics m, experimental observations indicate that eigenmodes are more nearly composed of a single-m harmonic.[21]

The stochastic transition for the alphas is illustrated by the sequence of orbits in Fig. 3c and Fig. 5. The radial variation in time at $\alpha_{mx} = .4 \times 10^{-3}$ (Fig. 5c) has the regular sinusoidal character of a nonstochastic 'superbanana' orbit, and is confined after 1000 transits, while that for $\alpha_{mx} = .6 \times 10^{-3}$ (Fig. 5b) appears less regular, and escapes within 100 transits. Thus, the stochastic threshold appears to lie around $\alpha_{mx} = .5 \times 10^{-3}$, or, since the chosen initial conditions do not allow the particle to reach $r = r_{mx}$,

perhaps somewhat lower.

The appearance of this new set of islands may be understood as follows. Similar analyses for passing particles have been done independently in Ref. 10 for $\omega = 0$, and in Ref. 9 in the higher–frequency TAE–mode case. Here ω is left arbitrary, as a first step in the extensions of the theory discussed in Sec. III. The radial drift $\dot{\bar{r}}$ of the particle's bounce–averaged radius $\bar{r}$ is given from Eq.(2) by

$$\dot{\bar{r}} = -v_{\|} b(r) \cos\eta. \tag{4}$$

For phase variable z equal to any of $r, v_{\|}, \theta, \zeta$ or η, one can express z in terms of the bounce phase θ_b as $z(\theta_b) = \bar{z}(\theta_b) + \delta z(\theta_b)$, where $\delta z(\theta_b)$ is a portion oscillatory at the bounce frequency, with zero bounce-average, and $\bar{z}$ is the 'bounce–averaged' portion. For $z \to \theta, \zeta$, or η, $\bar{z}$ evolves linearly in time or θ_b, while for $z \to r$ or $v_{\|}$, $\bar{z}$ is a constant. For particles not too near the trapped/passing boundary, δz may be approximated as purely sinusoidal. Thus, for both trapped and passing particles ($\tau = 0$ and 1), one has:

$$\begin{aligned} r &\simeq \bar{r} + r_1 \cos\theta_b, \\ v_{\|} &\simeq \tau u_0 + u_1 \cos\theta_b \\ \theta &\simeq \tau\theta_b + \theta_1 \sin\theta_b, \\ \zeta &\simeq (\Omega_\zeta/\Omega_b)\theta_b + \zeta_1 \sin\theta_b. \end{aligned} \tag{5}$$

Inserting these into the $\cos\eta$ factor in Eq.(4), one has

$$\cos\eta = \sum_l J_l(\eta_1) \cos\eta_l, \tag{6}$$

where the $J_l \equiv J_l(\eta_1)$ are Bessel functions, $\eta_l \equiv \bar{\eta} + l\theta_b \equiv n\bar{\zeta} + (l - \tau m)\theta_b + \phi_{nm}$, and amplitude $\eta_1 \equiv n\zeta_1 - m\theta_1$ is one half the change in mode phase

during a bounce/transit time due to the oscillatory portion of the motion. If one in addition assumes that mode amplitude $b(r)$ changes little over the scale of the particle banana width r_1, one may write $b(r) \simeq b(\bar{r}) + \delta r \partial_r b \equiv b_0 + b_1 \cos\theta_b$. Inserting this expression for $b(r)$ and Eq.(6) into Eq.(4), and gathering terms in η_l, one obtains

$$\dot{\bar{r}} = -\sum_l v_l \cos\eta_l, \tag{7}$$

with amplitudes v_l given by

$$\begin{aligned} v_l &= (\tau u_0 b_0 + u_1 b_1/2) J_l \\ &\quad + ((\tau u_0 b_1 + u_1 b_0)(J_{l-1} + J_{l+1}) + (u_1 b_1/4)(J_{l-2} + J_{l+2}). \end{aligned} \tag{8}$$

It should be noted that expression (7) is quite general, while expression (8) for v_l is only approximate. Other limits one might want to consider, for example, r_1 large compared to the mode width rather than small, present no difficulty for the basic formalism (see, for example, Ref. 17).

The origin of the appearance of the additional $m = 3$ islands in Fig. 4b may be seen from the $l = -1$ ($l_b = -3$) sideband contribution in Eq.(7). The $l = 1$ sideband is also present, and would contribute at the $q = 1$ surface. For the present parameters, however, this surface lies near $r = 0$, where the strength of the (2,1) perturbation has become negligible. In the limit of zero energy, $\eta_1 \to 0$, and $J_l \to \delta_{l0}$, with δ_{ij} the Kronecker delta. If (as is the case for present parameters) u_1 and b_1 are also small, in this limit only the $l = 0$ contribution, producing the driftless, magnetic island, survives. To complete the analysis, we need the equation for the time–development of the phases η_l. This is given by

$$\Omega_l \equiv \dot{\eta}_l = n\Omega_\zeta + l_b\Omega_b - \omega \simeq [n + l_b/q(r)]\Omega_\zeta - \omega. \tag{9}$$

(The final form holds only for $\tau = 1$.) Taking only a single l contribution in Eq.(7) along with Eq.(9), and expanding Ω_l as usual about the resonant surface q_l where $\Omega_l = 0$, one obtains an expression for the island half-width for the l^{th} surface:

$$\delta r_l / R = (4v_l/\Omega_l')^{1/2} = (4qb_0 G_l / nRq')^{1/2}. \tag{10}$$

Again, the final form holds only for passing particles, for which $\Omega_l' \equiv \partial_r \Omega_l \simeq n\Omega_\zeta(q'/q)$, and we have written $v_l \equiv u_0 b_0 G_l$, with the 'coupling coefficients' G_l, normalized so that they are dimensionless, and approximately given by Bessel functions J_l. These are plotted in Fig. 6a versus η_1, for three values of pitch angle $\chi \equiv \arccos\lambda$, $\chi = 0.0, 0.1$, and 0.2, ranging from deeply passing to only moderately passing particles. One notes the insensitivity of the curves to χ, consistent with the numerical observation made earlier.

The stochasticity threshold is given by the condition that adjacent island widths overlap,

$$\delta r_{l+1} + \delta r_l \gtrsim r_{l+1} - r_l, \tag{11}$$

where $r_l \equiv r(q_l)$, and δr_l is given in Eq.(10). Using the G_l from Fig. 6a in Eq.(10), in Fig. 6b we plot the island boundaries $r_l \pm \delta r_l$ for the $l = 0$ and -1 islands again versus η_1, for the same three values of χ, and for $\alpha_{mx} = .5 \times 10^{-3}$. One sees that the sideband (3,1) island overlaps the primary (2,1) island for η_1 greater than about 6.5, corresponding to an energy $E \simeq .45 E_0$. Because the island width curves are rather flat at and above this energy, the analytic overlap threshold for $E = E_0$ is also around $\alpha_{mx} = .4 - .5 \times 10^{-3}$, agreeing with the numerically-inferred value from Fig. 5.

$\alpha_{mx} \simeq .5 \times 10^{-3}$, or $b_{mx} \simeq 4 \times 10^{-3}$ is a large value for an MHD perturbation. TAE modes on DIII-D and TFTR are observed[22] to reach amplitudes

b of 1 to a few times 10^{-3}, and comparable values have been observed for fishbones on PDX.[23] For low–ω, low–n perturbations, the inferred interior amplitudes observed are somewhat smaller, $b \simeq .4 - .5 \times 10^{-3}$.[21] Thus it appears likely that the stochastic threshold $b_{mx} = b_{st} \simeq 4 \times 10^{-3}$ is somewhat larger than values realized experimentally. However, since b_{st} is not too much larger than values believed to be produced experimentally, a number of points should be noted. First, as n increases, b_{st} falls off weakly, $b_{st} \sim n^{1/2}$. (However, this trend should be offset by the fact that experimental fluctuations also fall off with n.) The presence of multiple harmonics can also act to reduce the required threshold, as implied by the extended theory of Sec. III. Caution in the conclusion that experiments are below threshold is also recommended by experimental measurements. As noted in Sec. I, it has been observed on TFTR[13] that the additional MHD–induced flux Γ_p, believed to arise principally from counter-going passing tritons making their way across the passing/trapped boundary and thereby exiting, is a factor of about 3 times the quiescent 'prompt' flux Γ_t, which derives principally from particles born trapped, which are lost to the detector during their first bounce period. Assuming conservation of E and magnetic moment μ, the maximum possible value Γ_p^{mx} of Γ_p is the number of counter-going particles born per unit time which make their passing/trapped transition at the minor radius r_d necessary to hit the TFTR triton/alpha detector. An estimate of the ratio Γ_p^{mx}/Γ_t yields[24] about 2.5 for a 1.8 MA case, roughly the experimental value of 3, suggesting that, in the presence of MHD, passing particles from all minor radii interior to r_d make their way rapidly to the passing/trapped boundary. Were passing particles only able to make small, nonsecular radial superbanana excursions δr_{sb} due to the MHD, as

one expects below threshold, Γ_p/Γ_t would be smaller by a factor of at least $\delta r_{sb}/r_d \ll 1$.

III. Extended Theory

The agreement of the analytic and numerical results of the previous section provides some confidence in applying the same analytic approach to more complicated situations of interest. It is also desirable to put the theory in a form where its connection to instances of stochastic transport which have been studied earlier is clarified.

The generalization to arbitrary ω has already been carried out in the single–harmonic development in Sec. II. An important further extension we wish to make on the theory of Sec. II is to allow for the presence of multiple harmonics. Each harmonic component, which we designate with harmonic label a, has its own values of $(m,n)_a$, and phase ϕ_a.

The stochastic mechanism of principal interest in this paper is for $\tau = 1$ particles, with perturbed radial motion $\dot{\tilde{r}} = \dot{\tilde{r}}_A$ given in Eq.(4), arising from the parallel portion $A_\parallel \equiv \tilde{\alpha} B_0 R_0$ of the vector potential. In contrast, the original case of tokamak stochastic transport studied[5] was for $\tau = 0$ particles, perturbed by radial 'grad-B' drifts $\dot{\tilde{r}}_B$ from TF coil ripple. In the general case, one might also wish to include a further transport mechanism, *viz.*, the contribution $\dot{\tilde{r}}_E$ to $\dot{\tilde{r}}$ arising from electrostatic perturbations. At little extra formal cost, the treatment of all these mechanisms may be combined.

Expression (1) for $\tilde{\alpha}$ or $A_\parallel$ is generalized in the obvious way, $\tilde{\alpha} = \sum_a \alpha_a(r) sin\eta_a$. Similarly, we write the magnetic ripple strength $\tilde{\delta}(\mathbf{x}) \equiv$

$\delta B(\mathbf{x})/B_0$ as $\tilde{\delta}(\mathbf{x}) = \sum_a \delta_a(r) sin\eta_a$. (For simplicity, the relative phases of the components of $\tilde{\alpha}$ and $\tilde{\delta}$ are taken equal to 0.) For $\dot{\tilde{r}}_E$, an analogous expression may be used for the perturbing potential $\tilde{\phi}$. For alphas, however, this effect is negligible, and so will be dropped here. Then a single expression for $\dot{\tilde{r}}$, valid for both $\tau = 0$ and 1 particles, including both the $A_\parallel$ and grad-B mechanisms, and multiple harmonics, is

$$\begin{aligned}
\dot{\tilde{r}} &= \dot{\tilde{r}}_A + \dot{\tilde{r}}_B = \sum_a [-v_\parallel b_a(r) + \hat{v}_{Ba}] \cos\eta_a \qquad (12)\\
&\simeq -\sum_{l_b}\sum_a [(ru_0b_0 - \hat{v}_B)_a J_{l_a} \\
&\quad + \frac{1}{2}(ru_0b_1 + u_1b_0)_a (J_{l_a-1} + J_{l_a+1})] \cos(n_a\bar{\zeta} + l_b\theta_b + \phi_a) \\
&= -\sum_{n_a}\sum_{l_b} v_{l_b} \cos(n_a\bar{\zeta} + l_b\theta_b + \phi_b).
\end{aligned}$$

Here, $l_a \equiv l_b + \tau m_a$, each of the Bessel functions has argument $\eta_{1a} \equiv n_a\zeta_1 - m_a\theta_1$, generalizing the earlier definition of η_1 in the obvious way, and $\hat{v}_{Ba} \equiv qn_a\mu\delta_a/(M\Omega_g r)$ is the amplitude of the grad-B drift due to component a. Ω_g is the particle gyrofrequency, and M its mass. In the third form given (second and third lines), we have neglected terms of order u_1b_1. Writing the summation over $a \rightarrow (m_a, n_a)$ in this form as $\sum_{(m_a,n_a)} v_{l_a} \cos(n_a\bar{\zeta}+l_b\theta_b+\phi_a)$, in the final form, we gather the summation over m_a into the definitions of the overall harmonic amplitudes v_{l_b} and phases ϕ_b, given by $v_{l_b}^2 \equiv v_{cl}^2 + v_{sl}^2$ and $\tan(\phi_b) \equiv v_{sl}/v_{cl}$, where $v_{cl} \equiv \sum_{m_a} v_{l_a} \cos\phi_a$, and $v_{sl} \equiv \sum_{m_a} v_{l_a} \sin\phi_a$. If one assumes all harmonics have just a single n_a, as is the case, for example, for fully toroidal eigenmodes, the resultant final expression for $\dot{\tilde{r}}$ is formally the same as the single–harmonic, single–mechanism expression (7). As a result, Expression (10) for the island widths is still valid, as is stochasticity criterion (11), with the simple replacement $v_l \rightarrow v_{l_b}$. With the sum

over n_a retained, Eq.(12) is formally the same as that used by Stix[25] and by Rechester and Rosenbluth[26] to study the driftless 'magnetic braiding' problem (though the perturbations envisioned there were higher–n), where the summation $\sum_{l_b}$ here replaces $\sum_{m_a}$ there, and reduces to it in the driftless limit.[16]

A. Connection with Other Stochastic Mechanisms

With Eq.(12) in hand, we digress briefly from the low-ω, $\tau = 1$ mechanism on which this work mainly focusses, and consider the relationship of that mechanism to the other stochastic mechanisms already mentioned.

The relationship to the high-ω, $\tau = 1$ case[8,9] is straightforward. Assuming $\dot{\bar{r}} = \dot{\bar{r}}_A$ and considering a single harmonic, Eq.(12) reduces to (7), and it and (9) are valid for arbitrary ω. Thus, from Eq.(9), as ω is changed from 0, the principal change is a shift in the positions $q_l(\tau = 1) \simeq (\omega/\Omega_b - l_b)/n$ of the resonant surfaces from their 0–frequency values $-l_b/n$, with the island widths δr_l and resultant overlap condition varying only slowly with equilibrium parameters. Thus, a shift $\Delta\omega = \Omega_b$ in ω moves the resonant surfaces radially across the spacing $\Delta_1 q \equiv q_l - q_{l+1} = 1/n$ between two successive rational surfaces. In the case of Fig. 4b, this would shift the primary ($l = 0$) island from the $q = 2$ to the $q = 3$ surface, where the $l = -1$ island now stands, and move an $l = 1$ island of comparable width to the $q = 2$ surface, leaving the overlap condition across the $q = 2$ and 3 surfaces about the same. Since $\omega \sim \Omega_b$ for the TAE modes, one expects a shift of about this size in the resonant surfaces, and accordingly small changes in the stochasticity threshold.

For frequency shifts somewhat larger than this, since the island widths δr_l fall off as $|l|$ increases, the wider, primary islands can be shifted out of the range of q in the plasma, and the stochastic mechanism can thereby be eliminated. An analogous frequency-dependent 'quenching' of the trapped-particle stochastic mechanism has also been found analytically[4] and corroborated numerically.[18]

One noteworthy singular feature of the $\omega = 0$ problem is that $q_l(\omega = 0)$ is independent of particle quantities. Thus, while all particles have the same set of q_l for $\omega = 0$, for $\omega \neq 0$ the rational surfaces shift from the $\omega = 0$ positions at rates depending on the particle energy and pitch, *via* Ω_b. This will introduce a greater sensitivity of stochasticity to pitch λ than that observed above for the $\omega = 0$ case. This may make low-w perturbations preferable in the context of the ash removal process to be discussed in Sec. IV.

The relation of the $\tau = 1$ mechanism to that for $\tau = 0$[3-5] is not quite as simple, because η_1 is a more sensitive function of $\bar{r}$ for $\tau = 0$ than for $\tau = 1$. Specializing Eq.(12) to $\tau = 0$ and to the single-harmonic, $\dot{\bar{r}} = \dot{\bar{r}}_B$ case for which the $\tau = 0$ problem has been studied, one has expression (7) (as for $\tau = 1$), now with $v_l = -\hat{v}_B J_l$.

For $\tau = 1$, $\eta_1 \simeq -m\theta_1$ depends principally upon perpendicular drifts, which change only weakly with $\bar{r}$. Thus, for $\tau = 1$, J_l remains about constant as $\bar{r}$ changes, the principal radial variation in the problem entering through $\Omega_l(\bar{r})$ in Eq.(9). This results in the resonant island width δr_l given in Eq.(10). Referring to this width for the moment as $\delta_1 r$, and to the radial spacing between successive resonances as $\Delta_1 r = \Omega_b/\Omega_l' \simeq 1/(nq')$, overlap condition (11) may be approximately written $\delta_1 r \gtrsim \Delta_1 r$.

In contrast, for $\tau = 0$, changes in $\bar{r}$ produce large changes in the particle

turning point θ_1 (a quantity determined by parallel motion), and thus in $\zeta_1 \simeq q\theta_1$ and $\eta_1 \simeq qN\theta_1$. (Here, $qN \equiv qn - m = qRk_\parallel$.) Now, when a particle drifts radially a distance $\Delta_2 r = \pi/\partial_r \eta_1 \simeq \pi/(nq'\theta_1)$, the change in η_1 is large enough to cause J_l or v_l to reverse sign. Thus, for $\Delta_2 r < \Delta_1 r$, as is typically the case for $\tau = 0$, each resonance does not produce a single island of width $\Delta_1 r$, but a series of 'sub-islands,' of width $\Delta_2 r$, with separatrices coming at the successive zeroes of the J_l for that resonance. Stochasticity then ensues when the *non*resonant excursion $\delta_2 r = v_{l\pm1}/\Omega_b$ induced by the neighboring harmonics is large enough to push a particle from one sub-island to the next, *i.e.* $\delta_2 r \gtrsim \Delta_2 r$. Using the expressions just given for these widths, along with the large-argument form $J_l(z) \sim 1/\sqrt{\pi z}$ and taking $\theta_1/\pi \sim 1$ results in the stochasticity criterion of Ref. 5, up to a numerical factor.

A final stochastic mechanism previously studied, both in the absence,[25,26] and presence[16] of particle drifts, is transport in the presence of multiple, high–n harmonics. The same theory as in Ref. 16 also applies to the present low to moderate–n case. Because for multiple n the q_{nm} can fall in an interlacing pattern, island overlap can occur at lower amplitudes than given by (11) for the single–n problem. Numerical corroboration for this has recently been given by Hsu and Sigmar for the TAE–problem:[27] while $b_{st} \sim 10^{-3}$ for a single $n \sim 1$ eigenmode, for multiple n, $b_{st} \sim 10^{-4}$ is found.

IV. Energy–Selective Transport

We now wish to investigate some of the possibilities raised by the extended theory of the previous section. Expression (12), along with the definitions of v_{l_b} and ϕ_b, make explicit the way in which multiple harmonics

affect the island widths and consequent transport. One notes that both positive and negative interference of one mode with another is possible at each harmonic l_b, and, through the $J_{l_a}(\eta_{1a})$s, that this interference has an energy dependence which is not monotonic, as the intuitions discussed in Sec. I would suggest, but rather oscillatory.

In Figs.3 and 6b one sees the (2,1) mode inducing stochastic transport supporting the second of the two intuitions noted in Sec. I; more energetic particles become stochastic before less energetic particles (or magnetic field lines). However, it is easy to construct examples in which the opposite expectation is borne out. (Whether such perturbations are produced in the plasma by external windings, or by control of the current profile, or by some other means is beyond the scope of this paper. The intention here is only to explore what kinds of transport effects might be obtained, assuming the postulated perturbations can be produced.) In Fig. 7 is shown the effect on the island structure of adding to the (2,1) magnetic perturbation an additional (3,1) magnetic perturbation, having $\alpha_{m_2} = .125 \times 10^{-3}$. The (2,1) island width is not much changed. For the (3,1) island, however, the $l = -1$ sideband contribution from the (2,1) perturbation, proportional to J_{-1}, adds to the primary ($l = 0$) contribution $\propto J_0$ from the (3,1) perturbation, causing in this case a cancellation of the (3,1) island at $E/E_0 \simeq .5$. Thus, the 'stochasticity profile' has been reversed from that in Fig. 6b; while the (2,1) mode alone is below threshold for low–energy particles and stochastic for high–energy ones, for this (2,1)+(3,1) superposition energetic particles are nonstochastic while low–energy particles and the magnetic field itself are stochastic. It should also be noted that this result depends upon the relative phase $\phi_{31} - \phi_{21}$ between the perturbations. Were this phase shifted by π,

J_{-1} would instead *add* to the J_0, making particles of *all* energies shown stochastic.

For burn control, a stochasticity profile like that in Fig. 6 is desirable; one would like to remove energetic particles, which if left would cause thermal runaway, while not losing confinement of the bulk plasma. For ash removal, still another profile is needed; one still wants to be below threshold for the bulk, *as well as* for energetic alphas, but above threshold for alphas at some intermediate energy, where they have spent most of their energy in heating the plasma, but still have drift orbits making them distinguishable from the thermal background. For this one needs to make more use of the oscillatory character of the Bessel functions, and for that one needs a somewhat larger η_1, and so larger (m, n). Fig. 8 illustrates this, plotting the island boundaries for a $(6, 3)$ perturbation, with amplitude $\alpha_{mx} = .7 \times 10^{-4}$, or $b_{mx} = 1.7 \times 10^{-3}$. q_{nm} is thus the same as before, but η_1 can reach larger values. For this (m, n), the first zero of J_0, corresponding to the first null of the (6,3) island, falls approximately at $E = E_0$, putting that energy below threshold. And as E or η_1 approach 0, one is again below threshold, because one is near the zero of $J_{\pm 1}$ of the sideband islands. At intermediate energies, however, island overlap can occur, as one sees for the (6,3) and (7,3) islands, where overlap occurs in the range $[E_2, E_1] \simeq [.05, .4]E_0 = [.175, 1.4]$MeV.

A deficiency of the perturbation of Fig. 8 for purposes of ash removal is that it is radially local; the overlap occurs only in the vicinity of the rational surface $q_{nm} = 2$. To extend this to a range of radii, one can apply a superposition of harmonics a, each having a primary island at a sequence of q_{nm} extending over the minor radius, with each adjacent pair producing overlap patterns similar to that of Fig. 8. Again taking $n = 3$ and $\phi_a = 0$ for

all harmonics, with $m_0 \equiv 6$ yielding a primary island at $q_{nm} = 2$, in Fig. 9 we show an example of this. As in Fig. 8, the $(m,n) = (6,3)$ harmonic makes a contribution $\propto J_0$ to the $(-l_b, n) = (6,3)$ primary island at the $q = 2$ surface, and sideband contributions $\propto J_{\pm 1}$ to the (7,3) and (5,3) islands, as well as smaller contributions to higher-l sidebands. If one would superpose (7,3) or (5,3) harmonics, then each of these would contribute J_0's to the (7,3) and (5,3) islands, destroying the desired feature captured in Fig. 8 that the sideband island widths become small as the energy does. Thus, we superpose only every other $n = 3$ harmonic. Then, at the $q = 2$ surface, one has a superposition $.. + \hat{v}_{43}J_{-2} + \hat{v}_{63}J_0 + \hat{v}_{83}J_2 + .. \simeq \hat{v}_{63}J_0$, and at the $q = 5/3$ sideband surface, one has superposition $.. + \hat{v}_{43}J_{-1} + \hat{v}_{63}J_1 + ...$ In order that these two sideband contributions not tend to cancel, we see that one must choose successive harmonics to have alternating signs or, equivalently, one may take the ϕ_a's of successive harmonics to alternate between 0 and π. Thus, in Fig. 9 we have used $\alpha_{mx}(43) = -1.8 \times 10^{-4}$, $\alpha_{mx}(63) = .5 \times 10^{-4}$, and $\alpha_{mx}(83) = .35 \times 10^{-4}$, or $b_{mx}(43) = -3.4 \times 10^{-3}$, $b_{mx}(63) = 1.2 \times 10^{-3}$, and $b_{mx}(83) = 1.1 \times 10^{-3}$. One notes that as r decreases, the value of b_{mx} needed for overlap increases, because the lower shear at smaller r makes the spacing between rational surfaces larger. Also, for the present choice of perturbations, the maximum energy E_1 where overlap occurs becomes larger for the islands deeper in, because η_{1a} is decreasing. Thus, while $E_1 \simeq .4E_0$ for the overlap of the (6,3) island with the (7,3) or (5,3) islands, $E_1 \simeq .75E_0$ for the (5,3),(4,3) overlap. Thus, the perturbation represented in Fig. 9 would permit a broadening of the profile of still fairly energetic alphas from the plasma center, but would not create a channel for alpha loss further out until the alphas had slowed to energies more acceptable for ash removal. If

desired, a more constant value of E_1 might be achieved by raising the chosen m and n as q_{nm} is decreased.

V. Discussion

Summarizing, we have explored mechanisms of stochastic transport in tokamaks, focussing principally on the transport of passing MeV ions by low–frequency magnetic perturbations. It has been established numerically that, contrary to earlier belief, MHD perturbations can induce loss of energetic ions without concomitant loss of confinement of the bulk plasma. An analytic theory has been developed explaining this, and clarifying the connections among the stochastic mechanisms of earlier studies. The mechanism may explain observed MeV ion loss due to low–ω modes in TFTR, intermediate–ω activity on DIII-D, and connects smoothly with the loss mechanism for the higher–ω TAE modes seen on both machines. The theory also opens the possibility for creating beneficial effects, *viz.* burn control, ash removal, and perhaps compensating undesired transport effects of unavoidable, internally–produced perturbations.

From the initial explorations of the previous section, one sees that one has a good deal of flexibility in prescribing a perturbation yielding a desired stochasticity profile. For ash removal, one notes that n cannot be too small, or the first null of J_0 will not be reached near the alpha birth energy E_0. It also cannot be so large that the J_l go through several periods in going from $E = 0$ to E_0, since in that rapidly oscillatory limit, the ranges of the confined bands near $E = 0$ and $E = E_0$ become too narrow, both to confine thermal particles, and to confine alphas until they have provided sufficient

heating. For TFTR parameters, $n \simeq 3$ provided about the correct value. Since $\eta_1 \simeq -m\theta_1 \sim nr_1/a$, for larger machine size a, since banana width r_1 remains about constant, one needs larger n to keep η_1 in the proper range of a few times unity. The amplitudes of the perturbations needed are also quite large, which has the undesirable effect of losing too much of the plasma volume for confinement of thermal particles. A more refined use of multiple harmonics, which as has been noted can greatly diminish the needed amplitude for stochasticity, may help to alleviate this difficulty.

It is likely that the stochasticity profiles shown here can be improved upon by, for example, making the intermediate range over which overlap occurs more localized in energy, and further below threshold at other energies. Given the same argument η_1, the set of J_l's form a complete set, so one could in principal take a sum providing any shape island profiles $\delta r_l(E)$ one wished. However, the situation is complicated by the fact that the η_{1a}'s from successive harmonics are *not* the same, and also that the selection of amplitudes $\hat{v}_{mn}$ to tailor $\delta r_l(E)$ for one l fixes the form for the other l's. Nevertheless, one has an appreciable number of parameters which can be adjusted in attempting to provide a more optimal perturbation. Given some desired optimal form, the technological task of producing such a perturbation will clearly be quite challenging. However, comparable challenges, for example the design of similarly sophisticated fields for transport optimization in the stellarators Wendelstein-VII-AS and -VII-X, have proven readily achievable.

Acknowledgments

The author is grateful to E.D. Fredrickson, R. Kaita, R.B. White, and especially to S.J. Zweben for useful discussions relating to this work.

This work supported by U.S.Department of Energy Contract No.DE-AC02-76-CHO3073.

References

[1]K. McGuire, *et al.*, *Phys. Rev. Lett.* **50**, 891 (1983).

[2]R.B. White, R.J. Goldston,K. McGuire, A.H. Boozer, D.A. Monticello, and W. Park, *Phys.Fluids* **26**, 2958 (1983).

[3]H.E. Mynick, R.B. White, Theory of Fusion Plasmas, International School of Plasma Physics, October, 1988, J. Vaclavik, F. Troyon, E. Sindoni (eds.) pp.385–400 (1989).

[4]H.E. Mynick and R.E. Duvall, *Phys. Fluids*–B 1, 750 (1989).

[5]R. J. Goldston, R. B. White and A. H. Boozer, *Phys. Rev. Lett.* **47**, 647 (1981).

[6]K.L. Wong, *et al.*, *Phys. Rev. Lett.* **66**, 1874 (1991).

[7]W. Heidbrink, *et al.*, *Nucl.Fusion* **31**, 1635 (1991).

[8]D.J. Sigmar, C.T. Hsu, R.B. White, C.Z. Cheng, (submitted to *Phys. Fluids–B*) (September, 1991).

[9]H. Ye, H.L. Berk, and B.N. Breizman, *Bull. Am. Phys. Soc.* **36**, paper 5S06 (1991).

[10]S.V. Konovalov, S.V. Putvinskii, *Sov. J. Plasma Phys.* **14**, 461 (1988).

[11]S.V. Konovalov, S.V. Putvinskii, *Fusion Technol.* **18**, 397 (1990).

[12]E. Bittoni, M. Haegi, Proc. IAEA Technical Committee Meeting on Alpha Particles, Gothenburg, Sweden (June, 1991).

[13]S.J. Zweben, R.E. Duvall, E.D. Fredrickson, R.J. Goldston, H.E. Mynick, J.D. Strachan, and R.B. White, *Phys. Fluids* **B2**, 1411 (1990).

[14]H.E. Mynick, Proc. 1992 Sherwood Theory Conference, paper 1C18 (Santa Fe, NM, April, 1992).

[15]H.H. Duong, "Confinement of MeV Ions in DIII-D," presented at the Third Workshop on Alpha Physics in TFTR, MIT, Cambridge, Ma (May, 1992).

[16]H.E. Mynick,J.A. Krommes, *Phys. Fluids* **23**, 1229 (1980).

[17]H.E. Mynick, J.D. Strachan, *Phys. Fluids* **24**, 695 (1981).

[18]R.E. Duvall, Ph.D. Dissertation, Princeton University (1990).

[19]A.H. Boozer, G. Kuo-Petravic, *Phys. Fluids* **24**, 851 (1981).

[20]R.B. White, M.S. Chance,*Phys. Fluids* **27**, 2455 (1984).

[21]E.D. Fredrickson, private communications (1992).

[22]W.W. Heidbrink and K.L. Wong, private communications (1992).

[23]D. W. Roberts, Ph.D. Dissertation, Princeton University (March, 1991).

[24]S.J. Zweben, R. Boivin, C.S. Chang, G. Hammett, H.E. Mynick, *Nucl. Fusion* **31**, 2219 (1991).

[25]T.H. Stix, *Phys. Rev. Lett.* **30**, 833 (1973).

[26]A. B. Rechester and M. N. Rosenbluth, *Phys. Rev. Lett.* **40**, 38 (1978).

[27]C.T. Hsu and D.J. Sigmar, presented at the Third Workshop on Alpha Physics in TFTR, MIT, Cambridge, Ma (May, 1992).

Figures

FIG. 1. Amplitudes $\alpha(r)$ for the model MHD perturbations, for (m,n) =(2,1), (3,2) and (1,1) modes.

FIG. 2. Poloidal projection of (a) one trapped ($\lambda = .18$) and (b) one passing ($\lambda = .46$) alpha orbit in TFTR, perturbed by a (2,1) mode with $\alpha_{mx} = 10^{-3}, \phi_{nm} = -\pi/2, \omega = 0$.

FIG. 3. Poloidal projection of several other passing orbits for the same perturbation and launch point as in Fig. 2. (a)$\lambda = .46, \phi_{nm} = 0$, (b)$\lambda = .46, \phi_{nm} = \pi/2$, (c)$\lambda = .6, \phi_{nm} = -\pi/2$, (d)$\lambda = -.46, \phi_{nm} = -\pi/2$.

FIG. 4. Poincare maps for (a) the magnetic field and (b) alphas with energy $E = 3.5$ MeV, and $\lambda = 1$, for a (2,1) mode with $\alpha_{mx} = 10^{-4}$.

FIG. 5. Sequence of orbits launched with same initial conditions as Fig. 3c ($r/R_0 = .15, \theta = -\pi/2, \zeta = 0, \lambda = .6, E = E_0$, and $(m,n) = (2,1), \phi_{nm} = -\pi/2$), but with perturbation amplitudes $\alpha_{mx}/10^{-3}$ = (a)0.7, (b)0.6, (c)0.4, and (e)0.1.

FIG. 6. (a) Plot of coupling coefficients G_l for $l = 0$ and -1 versus $\eta_1 \propto E^{1/2}$, for three values of pitch angle $\chi \equiv \arccos\lambda$, $\chi = 0.0, 0.1$, and 0.2. The marks on each curve are separated by $E_0/10$. (b) island boundaries for the $l = 0, -1$ islands versus η_1, using the G_l of Fig. 6a in Eq.(10), for $\alpha_{mx} = .5 \times 10^{-3}$.

FIG. 7. (a) profiles $\alpha_a(r)$ of a superposition of the same (2,1) mode of Fig. 6, along with an additional (3,1) perturbation with $\alpha_{mx} = .125 \times 10^{-3}$.

(b)Island boundaries for the superposition, assuming zero relative phase between the modes.

FIG. 8. Same plots as Fig. 7, but for a single (6,3) perturbation, with $\alpha_{mx} = .7 \times 10^{-4}$. Island overlap occurs for intermediate energies, but not for thermal energies or those near the alpha birth energy, as needed for ash removal.

FIG. 9. Extension of the ash removal approach of Fig. 8 to make it radially global, by superposing a series of harmonic perturbations, with $(m, n, \alpha_{mx}) = (4, 3, -1.8 \times 10^{-4}), (6, 3, .5 \times 10^{-4})$, and $(8, 3, -.35 \times 10^{-4})$.

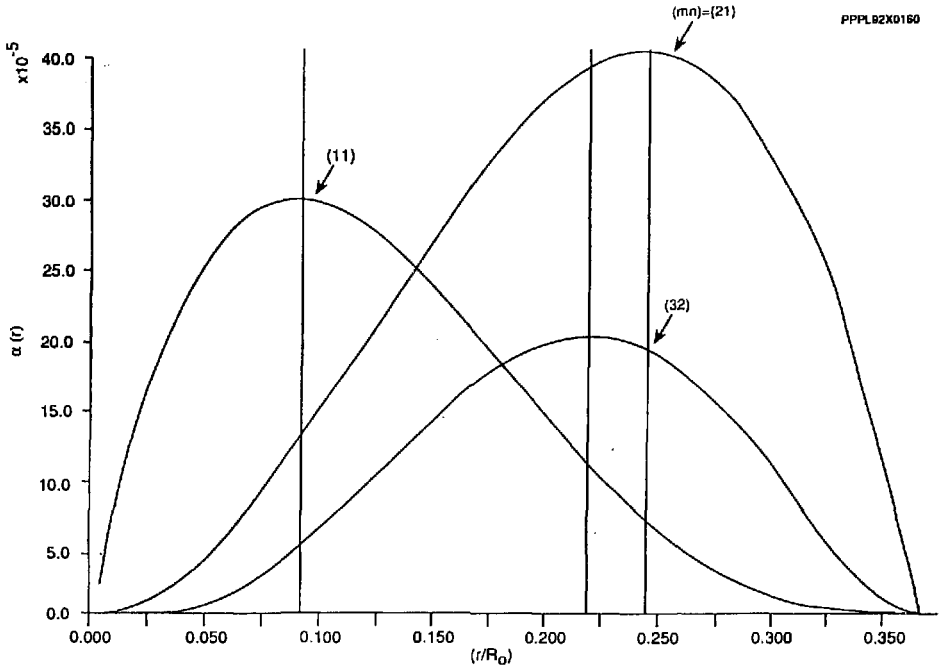
PPPL92X0160
(mn)=(21)
(11)
(32)
x10^-5
40.0
35.0
30.0
25.0
20.0
15.0
10.0
5.0
0.0
α (r)
0.000
0.050
0.100
0.150
0.200
0.250
0.300
0.350
(r/R0)

Fig. 1

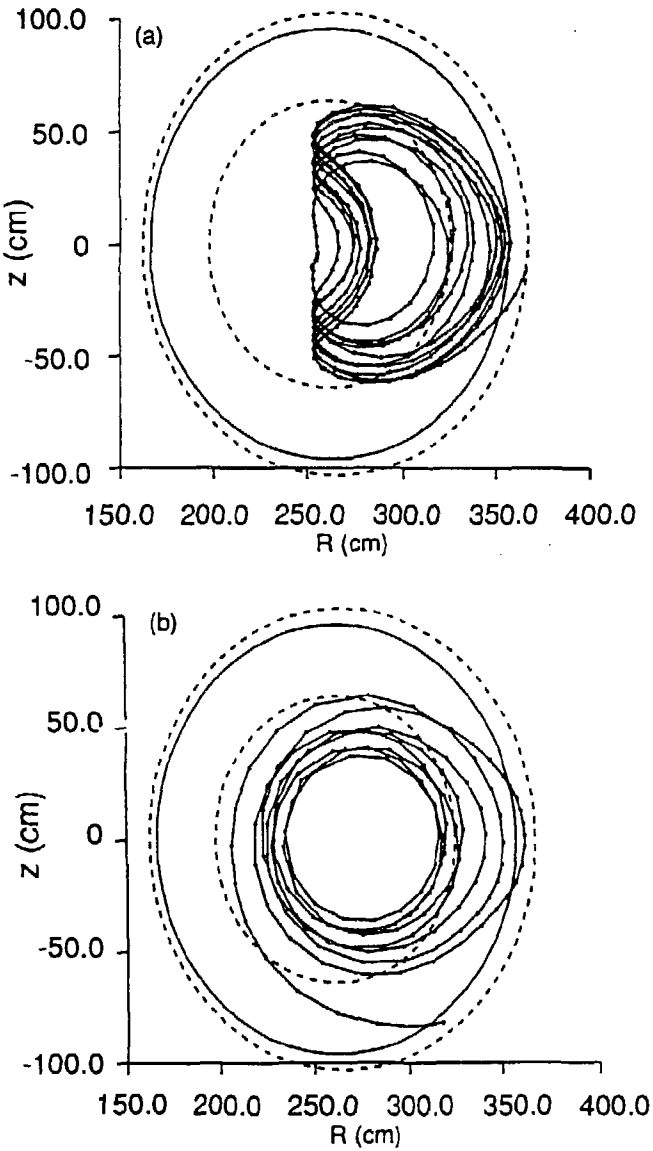
(a)
100.0
50.0
0
-50.0
-100.0
z (cm)
150.0 200.0 250.0 300.0 350.0 400.0
R (cm)
(b)
100.0
50.0
0
-50.0
-100.0
z (cm)
150.0 200.0 250.0 300.0 350.0 400.0
R (cm)

Fig. 2

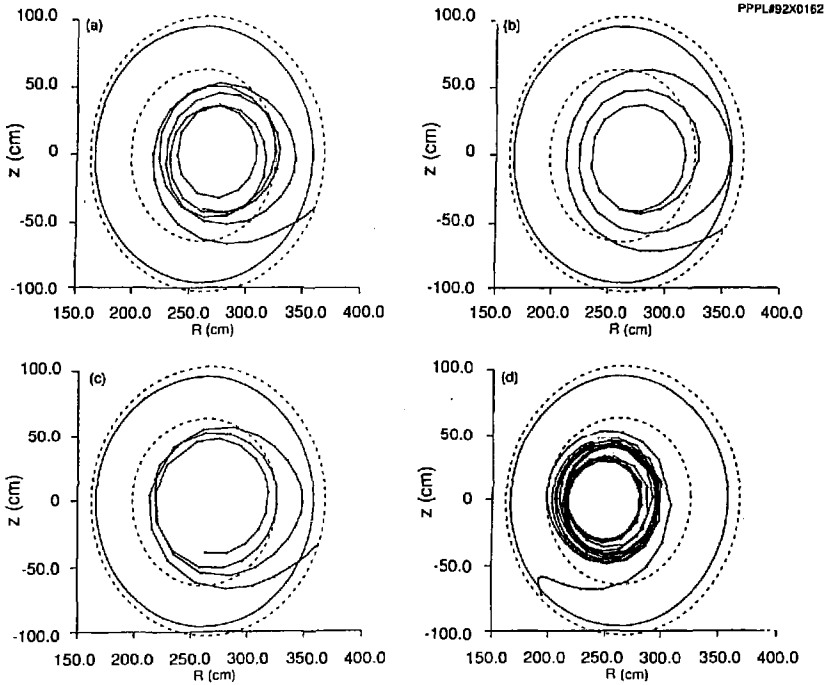
PPPL#92X0162
(a)
(b)
(c)
(d)
100.0
50.0
0
-50.0
-100.0
z (cm)
150.0 200.0 250.0 300.0 350.0 400.0
R (cm)

Fig. 3

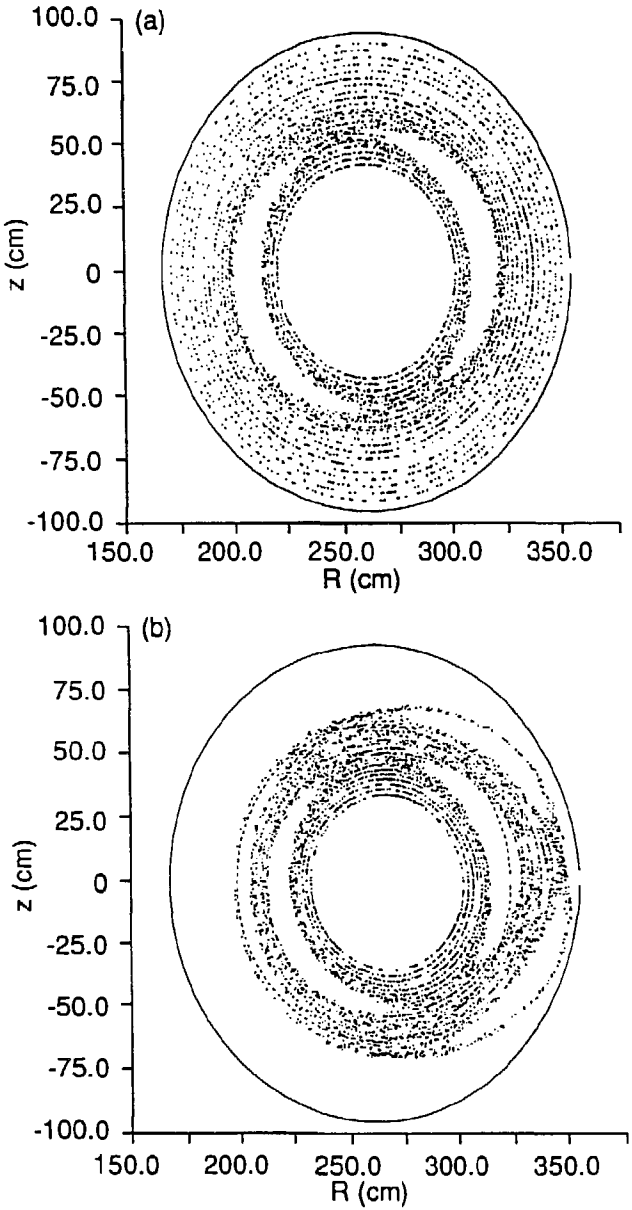
(a)
100.0
75.0
50.0
25.0
0
-25.0
-50.0
-75.0
-100.0
z (cm)
150.0
200.0
250.0
300.0
350.0
R (cm)
(b)
100.0
75.0
50.0
25.0
0
-25.0
-50.0
-75.0
-100.0
z (cm)
150.0
200.0
250.0
300.0
350.0
R (cm)

Fig. 4

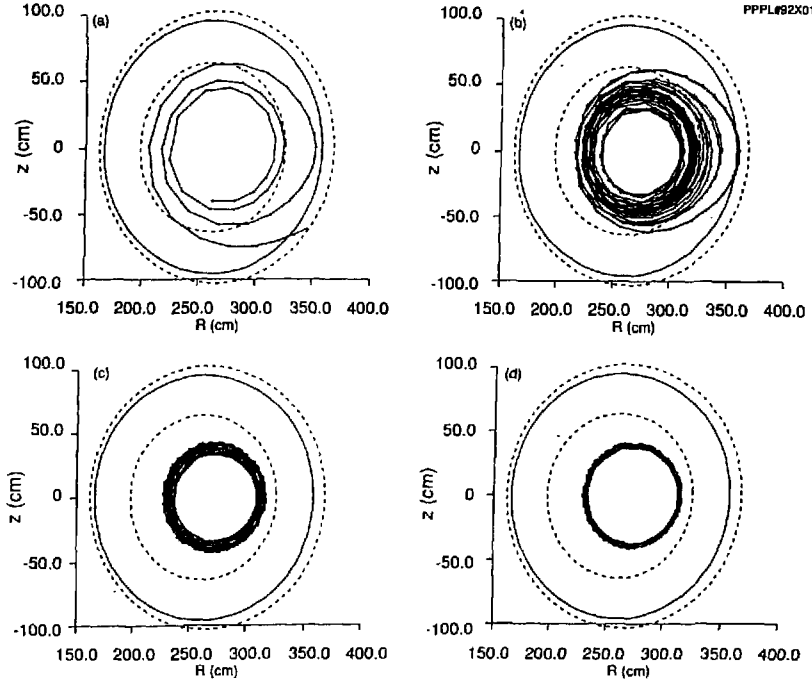
PPPL#92X0164
(a)
(b)
(c)
(d)
100.0
50.0
0
-50.0
-100.0
z (cm)
150.0 200.0 250.0 300.0 350.0 400.0
R (cm)

Fig. 5

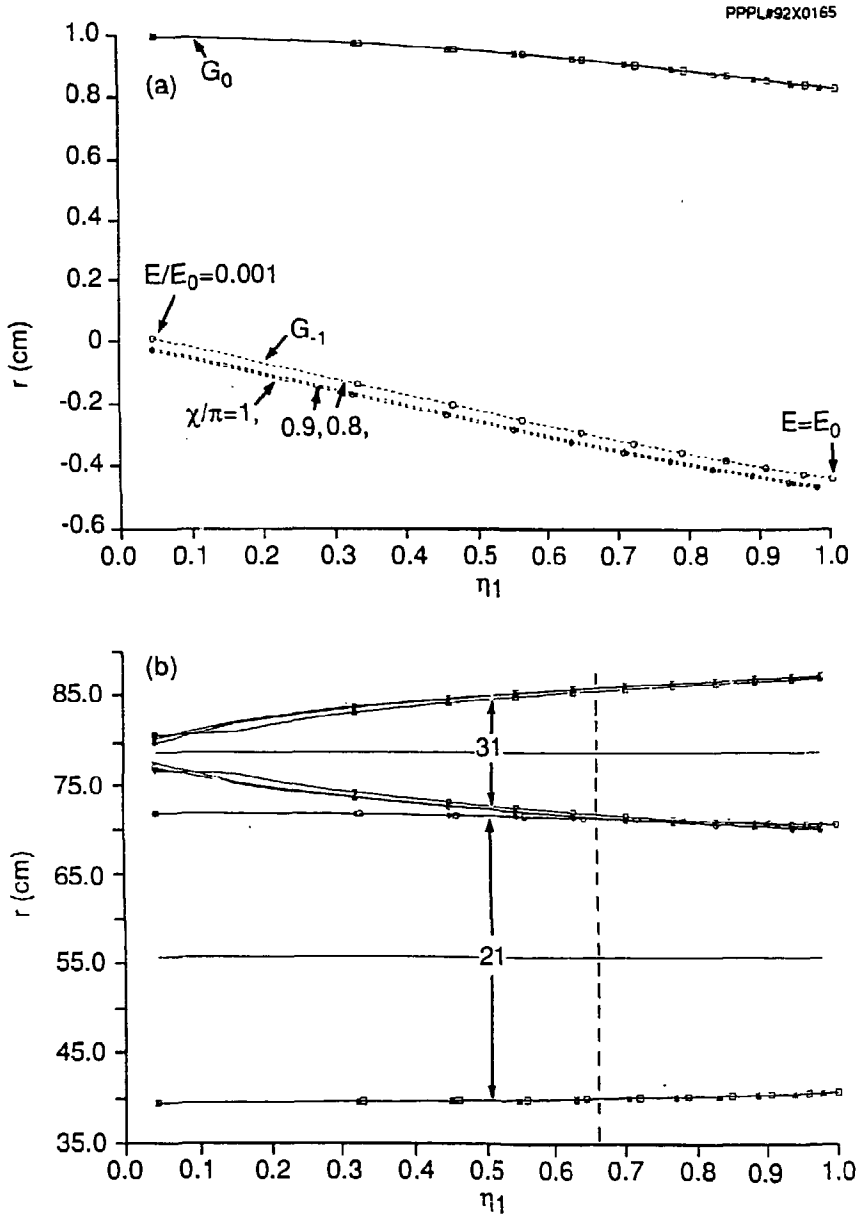
PPPL#92X0165
(a)
G_0
E/E_0=0.001
G_{-1}
χ/π=1,
0.9,0.8,
$E=E_0$
r (cm)
η_1
(b)
31
21
r (cm)
η_1

Fig. 6

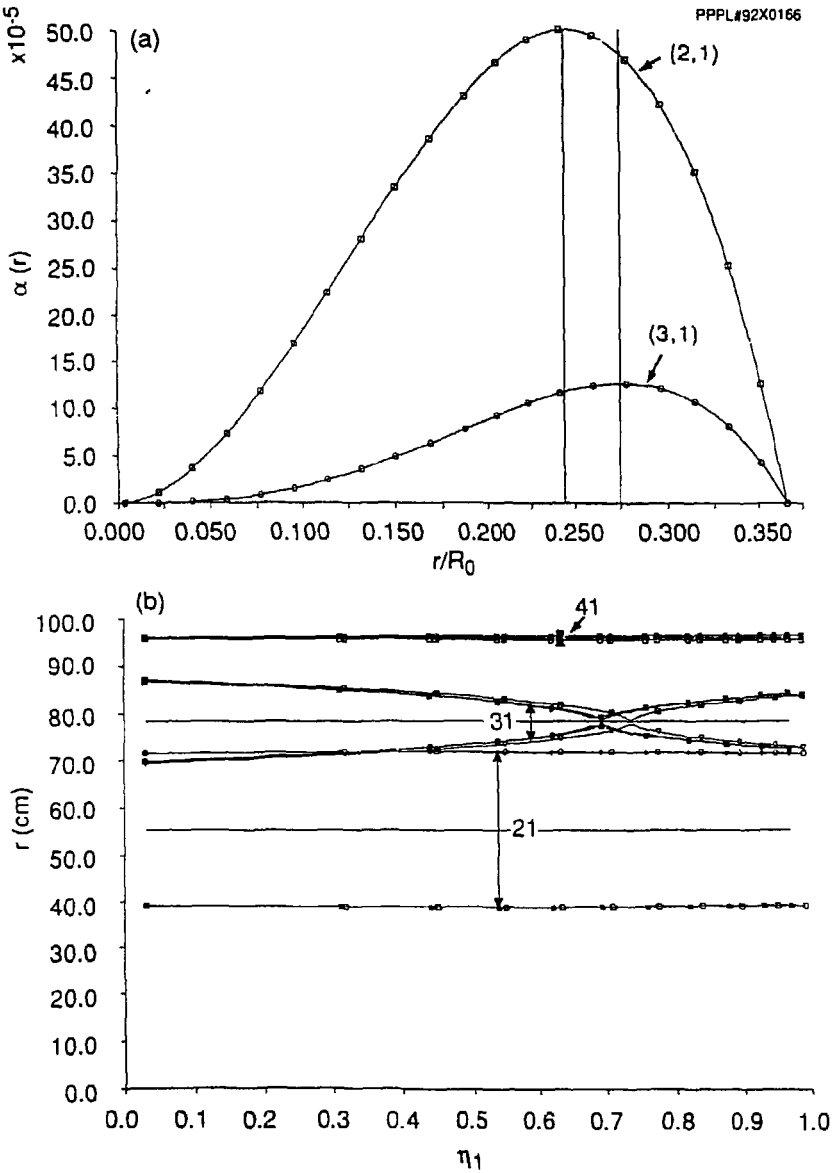

Fig. 7

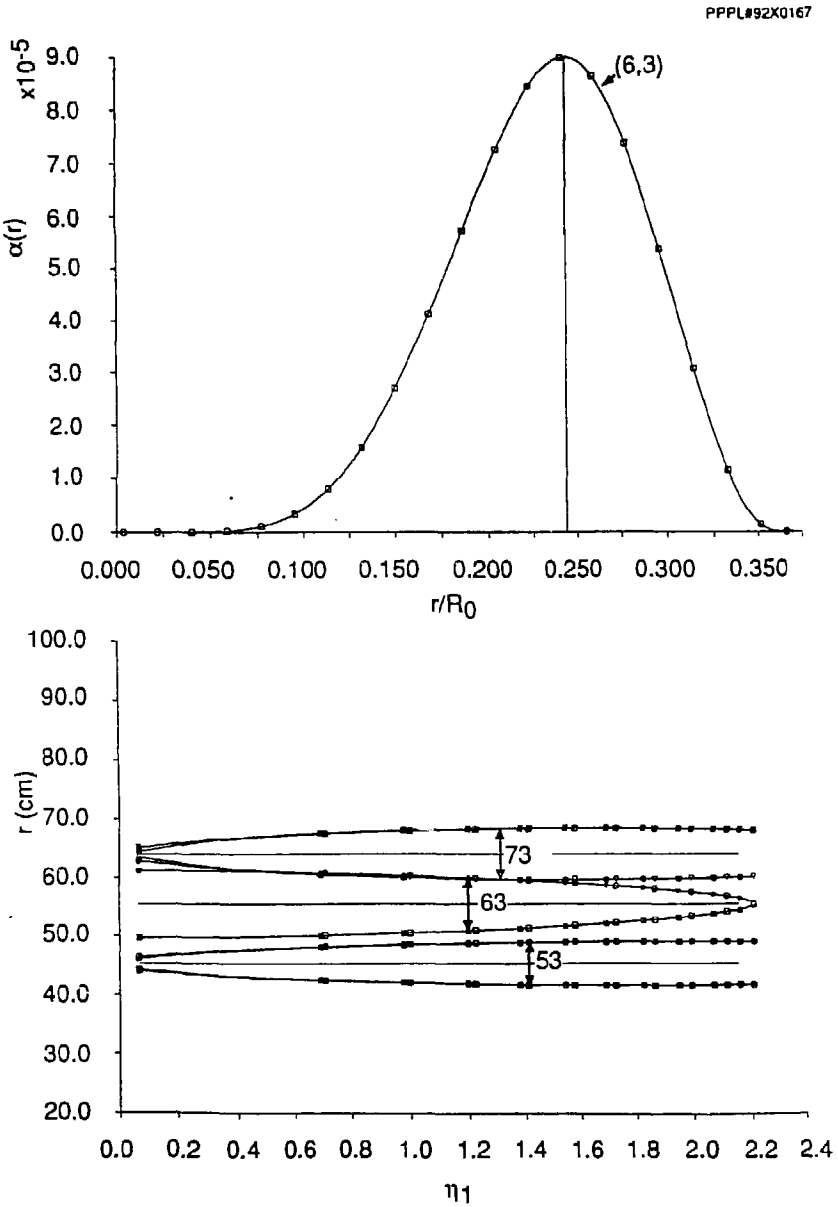
PPPL#92X0167
x10-5
α(r)
9.0
8.0
7.0
6.0
5.0
4.0
3.0
2.0
1.0
0.0
(6,3)
0.000
0.050
0.100
0.150
0.200
0.250
0.300
0.350
r/R0
r (cm)
100.0
90.0
80.0
70.0
60.0
50.0
40.0
30.0
20.0
73
63
53
0.0
0.2
0.4
0.6
0.8
1.0
1.2
1.4
1.6
1.8
2.0
2.2
2.4
η1

Fig. 8

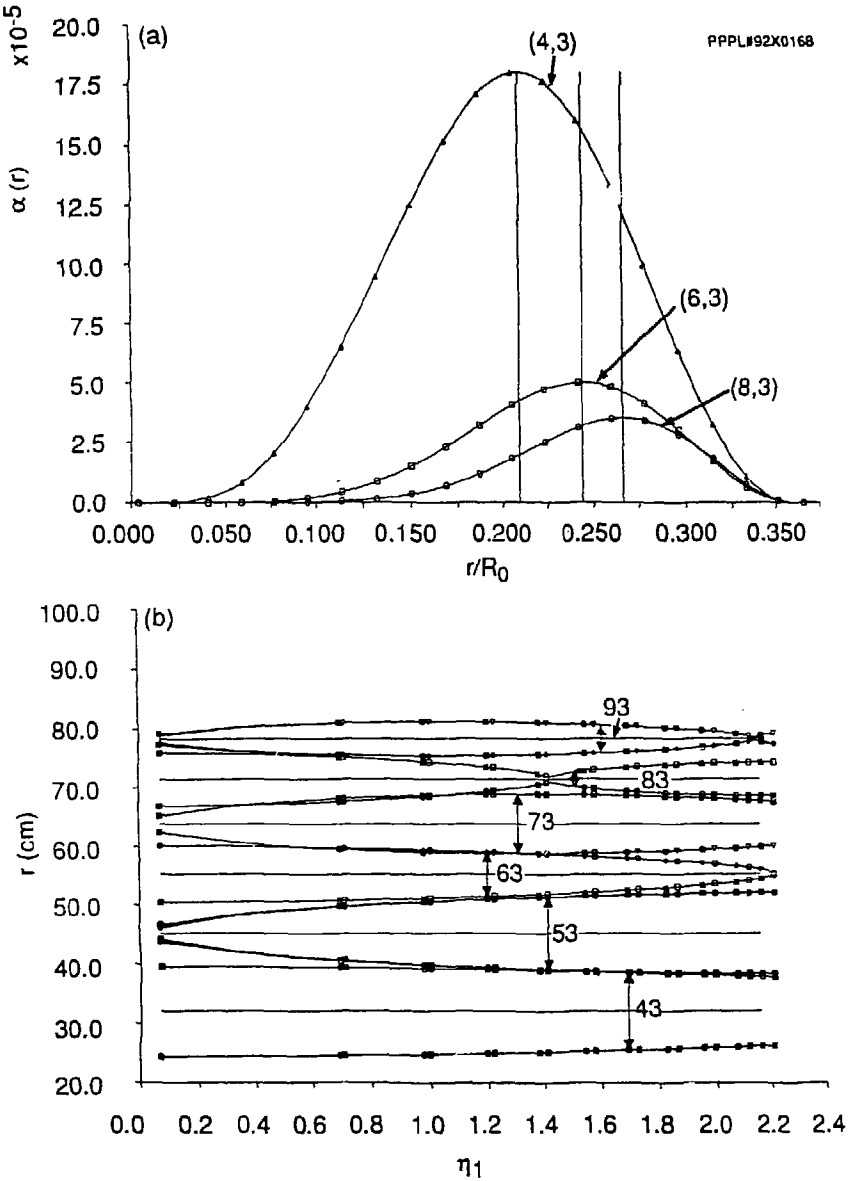

Fig. 9

EXTERNAL DISTRIBUTION IN ADDITION TO UC-420

Dr. F. Paoloni, Univ. of Wollongong, AUSTRALIA
Prof. M.H. Brennan, Univ. of Sydney, AUSTRALIA
Plasma Research Lab., Australian Nat. Univ., AUSTRALIA
Prof. I.R. Jones, Flinders Univ, AUSTRALIA
Prof. F. Cap, Inst. for Theoretical Physics, AUSTRIA
Prof. M. Heindler, Institut für Theoretische Physik, AUSTRIA
Prof. M. Goossens, Astronomisch Instituut, BELGIUM
Ecole Royale Militaire, Lab. de Phy. Plasmas, BELGIUM
Commission-European, DG. XII-Fusion Prog., BELGIUM
Prof. R. Boucique, Rijksuniversiteit Gent, BELGIUM
Dr. P.H. Sakanaka, Instituto Fisica, BRAZIL
Instituto Nacional De Pesquisas Espaciais-INPE, BRAZIL
Documents Office, Atomic Energy of Canada Ltd., CANADA
Dr. M.P. Bachynski, MPB Technologies, Inc., CANADA
Dr. H.M. Skarsgard, Univ. of Saskatchewan, CANADA
Prof. J. Teichmann, Univ. of Montreal, CANADA
Prof. S.R. Sreenivasan, Univ. of Calgary, CANADA
Prof. T.W. Johnston, INRS-Energie, CANADA
Dr. R. Bolton, Centre canadien de fusion magnétique, CANADA
Dr. C.R. James,, Univ. of Alberta, CANADA
Dr. P. Lukác, Komenského Universzita, CZECHO-SLOVAKIA
The Librarian, Culham Laboratory, ENGLAND
Library, R61, Rutherford Appleton Laboratory, ENGLAND
Mrs. S.A. Hutchinson, JET Library, ENGLAND
Dr. S.C. Sharma, Univ. of South Pacific, FIJI ISLANDS
P. Mähönen, Univ. of Helsinki, FINLAND
Prof. M.N. Bussac, Ecole Polytechnique,, FRANCE
C. Mouttet, Lab. de Physique des Milieux Ionisés, FRANCE
J. Radet, CEN/CADARACHE - Bat 506, FRANCE
Prof. E. Economou, Univ. of Crete, GREECE
Ms. C. Rinni, Univ. of Ioannina, GREECE
Dr. T. Mual, Academy Bibliographic Ser., HONG KONG
Preprint Library, Hungarian Academy of Sci., HUNGARY
Dr. B. DasGupta, Saha Inst. of Nuclear Physics, INDIA
Dr. P. Kaw, Inst. for Plasma Research, INDIA
Dr. P. Rosenau, Israel Inst. of Technology, ISRAEL
Librarian, International Center for Theo Physics, ITALY
Miss C. De Palo, Associazione EURATOM-ENEA , ITALY
Dr. G. Grosso, Istituto di Fisica del Plasma, ITALY
Prof. G. Rostangni, Istituto Gas Ionizzati Del Cnr, ITALY
Dr. H. Yamato, Toshiba Res & Devel Center, JAPAN
Prof. I. Kawakami, Hiroshima Univ., JAPAN
Prof. K. Nishikawa, Hiroshima Univ., JAPAN
Director, Japan Atomic Energy Research Inst., JAPAN
Prof. S. Itoh, Kyushu Univ., JAPAN
Research Info. Ctr., National Instit. for Fusion Science, JAPAN
Prof. S. Tanaka, Kyoto Univ., JAPAN
Library, Kyoto Univ., JAPAN
Prof. N. Inoue, Univ. of Tokyo, JAPAN
Secretary, Plasma Section, Electrotechnical Lab., JAPAN
S. Mori, Technical Advisor, JAERI, JAPAN
Dr. O. Mitarai, Kumamoto Inst. of Technology, JAPAN
J. Hyeon-Sook, Korea Atomic Energy Research Inst., KOREA
D.I. Choi, The Korea Adv. Inst. of Sci. & Tech., KOREA
Prof. B.S. Liley, Univ. of Waikato, NEW ZEALAND
Inst of Physics, Chinese Acad Sci PEOPLE'S REP. OF CHINA
Library, Inst. of Plasma Physics, PEOPLE'S REP. OF CHINA
Tsinghua Univ. Library, PEOPLE'S REPUBLIC OF CHINA
Z. Li, S.W. Inst Physics, PEOPLE'S REPUBLIC OF CHINA
Prof. J.A.C. Cabral, Instituto Superior Tecnico, PORTUGAL
Dr. O. Petrus, AL I CUZA Univ., ROMANIA
Dr. J. de Villiers, Fusion Studies, AEC, S. AFRICA
Prof. M.A. Hellberg, Univ. of Natal, S. AFRICA
Prof. D.E. Kim, Pohang Inst. of Sci. & Tech., SO. KOREA
Prof. C.I.E.M.A.T, Fusion Division Library, SPAIN
Dr. L. Stenflo, Univ. of UMEA, SWEDEN
Library, Royal Inst. of Technology, SWEDEN
Prof. H. Wilhelmson, Chalmers Univ. of Tech., SWEDEN
Centre Phys. Des Plasmas, Ecole Polytech, SWITZERLAND
Bibliotheek, Inst. Voor Plasma-Fysica, THE NETHERLANDS
Asst. Prof. Dr. S. Cakir, Middle East Tech. Univ., TURKEY
Dr. V.A. Glukhikh,Sci. Res. Inst. Electrophys.I Apparatus, USSR
Dr. D.D. Ryutov, Siberian Branch of Academy of Sci., USSR
Dr. G.A. Eliseev, I.V. Kurchatov Inst., USSR
Librarian, The Ukr.SSR Academy of Sciences, USSR
Dr. L.M. Kovrizhnykh, Inst. of General Physics, USSR
Kernforschungsanlage GmbH, Zentralbibliothek, W. GERMANY
Bibliothek, Inst. Für Plasmaforschung, W. GERMANY
Prof. K. Schindler, Ruhr-Universität Bochum, W. GERMANY
Dr. F. Wagner, (ASDEX), Max-Planck-Institut, W. GERMANY
Librarian, Max-Planck-Institut, W. GERMANY
Prof. R.K. Janev, Inst. of Physics, YUGOSLAVIA